Received: 5 July 2023 | *Revised:* 22 September 2023 | *Accepted:* 9 October 2023
DOI: 10.37917/ijeee.20.1.24 *Early View* | *June 2024*

Open Access

Iraqi Journal for Electrical and Electronic Engineering
Original Article

The Analysis of Sub-Synchronous Resonance in a Wind Farm for a Doubly-Fed Induction Generator Using Modern Analytical Method

Ali Kadhim Abdulabbas*[1], Shafaa Mahdi Salih[1], Mazin Abdulelah Alawan [2]
[1]Electrical Engineering Department, University of Basrah, Basrah, Iraq
[2]Department of Computer Science, Shatt Al-Arab University College, Basra, Iraq

Correspondance
*Ali Kadhim Abdulabbas
Electrical Engineering Department
University of Basrah, Basrah, Iraq
Email: ali.abdulabbas@uobasrah.edu.iq

Abstract
The occurrence of Sub-Synchronous Resonance (SSR) phenomena can be attributed to the interaction that takes place between wind turbine generators and series-compensated transmission lines. The Doubly-Fed Induction Generator (DFIG) is widely recognized as a prevalent generator form employed in wind energy conversion systems. The present paper commences with an extensive exposition on modal analysis techniques employed in a series of compensated wind farms featuring Doubly Fed Induction Generators (DFIGs). The system model encompasses various components, including the aerodynamics of a wind turbine, an induction generator characterized by a sixth-order model, a second-order two-mass shaft system, a series compensated transmission line described by a fourth-order model, controllers for the Rotor-Side Converter (RSC) and the Grid-Side Converter (GSC) represented by an eighth-order model, and a first-order DC-link model. The technique of eigenvalue-based SSR analysis is extensively utilized in various academic and research domains. The eigenvalue technique depends on the initial conditions of state variables to yield an accurate outcome. The non-iterative approach, previously employed for the computation of initial values of the state variables, has exhibited issues with convergence, lack of accuracy, and excessive computational time. The comparative study evaluates the time-domain simulation outcomes under different wind speeds and compensation levels, along side the eigenvalue analysis conducted using both the suggested and non-iterative methods. This comparative analysis is conducted to illustrate the proposed approach efficacy and precision. The results indicate that the eigenvalue analysis conducted using the proposed technique exhibits more accuracy, as it aligns with the findings of the simulations across all of the investigated instances. The process of validation is executed with the MATLAB program. Within the context of the investigation, it has been found that increasing compensation levels while simultaneously decreasing wind speed leads to system instability. Therefore, modifying the compensation level by the current wind speed is advisable.

Keywords
Sub-Synchronous Resonance, wind turbine, DFIG, eigenvalue-based SSR.

I. Introduction

A transmission line maximum transmittable power may be increased by installing a fixed series capacitor throughout its length. Nevertheless, one of the barriers influencing the use of series capacitive compensation widely in wind farms is the possible threat of SSR, impacting the stability and safety of the whole system [1]. An example of the SSR phenomenon is when a wind turbine using a DFIG is connected to a series-compensated network, and the two-systems trade energy at frequencies other than the fundamental frequency. SSR will

occur if the compensation level is high and the wind speed is low [2]. Induction Generator Effect (IGE) and Torsional Interactions (TI) are the two primary types of SSR.

In contrast to the IGE, which only involves the electrical part and how it interacts with the electrical network and generator, the TI effect has both electrical and mechanical parts [3]. The principal cause of Sub-Synchronous Resonance (SSR) in wind farms connected to a series compensated network is the network resonance oscillation mode, commonly referred to as IGE. Torsional modes in wind turbines have a frequency of 1-3 Hz because of the low shaft stiffness of the drive train; hence, it takes a very high amount of series compensation, which is uncommon, to generate TI [4]. As the IGE impact is the most pressing issue with current wind farms, it is the focus of this research.

Literature [5–10] has analyzed the SSR in series-compensated wind farms that use DFIGs. In these publications, we give a modeling and stability study of wind farms that use DFIGs and connect to the grid through a fixed-series compensated transmission line. According to [5, 6], the SSR might be useful for large wind farms that use double-cage induction generators connected to a fixed series-compensated line. It has been looked into [7–10] how well DFIG converters lower SSR in a fixed-series compensated DFIG-based wind farm. Time-domain simulation [5, 11], frequency-scanning [7, 12] , and eigenvalue analysis [9, 13] are only a few of the methodologies offered for SSR analysis. Several SSR studies [14–17] have used the latter strategy, making it the most prominent approach. However, 1) the authors have prioritized system modeling above, explaining the method of obtaining the initial values; 2) they have employed the iterative technique to compute the initial values; and 3) they haven't supplied nearly enough data to make the calculations meaningful. In [18], the authors propose an analytical method that has no assumptions, requires less computation time, is simple and easy to implement, takes into account the loss of the DFIG back-to-back converter, allows for non-zero reactive power delivery via the DFIG grid-side converter, and has no convergence problem. For this reason, the obtained starting values are reliable.

Several methods of analysis are utilized in this research to study SSR. The following are some critical contributions to this work:

1- Based on the eigenvalue technique, a new analytical strategy is provided for SSR analysis that is easy and accurate.

2- We build a complete model of a wind farm powered by DFIGs and connected to a series-compensated grid with MATLAB/Simulink.

3- The findings of a time-domain simulation are compared with those of an eigenvalue analysis based on the suggested and iterative approaches, and this is done for a range of wind speeds and compensation levels.

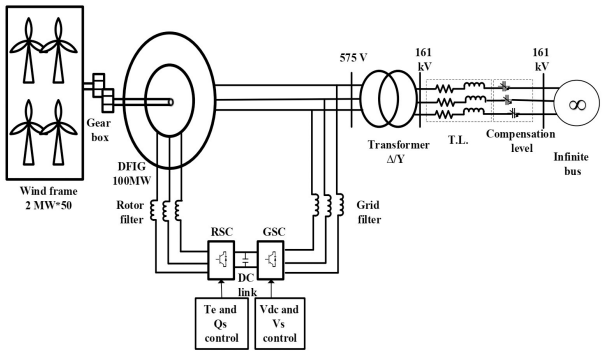

Fig. 1. Power system diagram for the proposed circuit.

The remaining sections of the paper are structured as follows: Section II. details introduces system modeling. In Section III. , the starting values of the state variables are determined. In Section IV. , we do an eigenvalue analysis. In Section V. , we provide our results from the SSR analysis. Section VI. provides the conclusion.

II. Electrical Power System Layout

1) Power Circuit

The infinite bus in this setup receives power from a 100 MW DFIG-based wind farm through a 161 kV series compensated transmission line. An installation of fifty 2-MW wind turbines would make up the 100-MW wind farm, as shown in Fig. 1 [14]. In this configuration, the whole power system is modelled. This includes the dynamic behaviour of the wind turbine aerodynamics, shaft system, induction generator (IG), Rotor Side Converter (RSC) controller, Grid Side Converter (GSC) controller, DC link, and series compensated transmission line. DFIG operates at 575 V and 60 Hz as its nominal voltage and frequency. The appendix contains the parameters for the single model and the aggregated model.

2) Analysis of Small-Signal Stability

The capacity of a system to remain stable in the presence of minimal perturbations is known as its small-signal stability. The small-signal stability study of a power system may help designers understand its intrinsic small-signal dynamic properties. A power system's behaviour may be described by a set of n first-order non-linear ordinary differential equations [19]. We could also be interested in the output variables, which may be written in terms of the state and input variables as follows:

$$\dot{x} = f(x, u) \tag{1}$$

$$y = g(x, u) \tag{2}$$

Where $x = [x_1,\ x_2, ..., x_n]^T$ is the state vector, and x_i are state variables. The inputs to the system are represented by the column vector $u = [u_1, u_2, ..., u_r]^T$ and $y = [y_1,\ y_2, ..., y_m]^T$ is the vector of outputs, and $g(x,u)$ is a vector of nonlinear functions; that relate outputs to inputs and state variables. It is possible to represent the dynamics of the system in state-space form by linearizing the differential equations (1) and (2) around an operational point, as long as the disturbances to the system are assumed to be small as shown in (3) .

$$\begin{aligned} \Delta\dot{x} &= A\Delta x + B\Delta u \\ \Delta y &= C\Delta x + D\Delta u \end{aligned} \tag{3}$$

3) Aerodynamics of Wind Turbines

From the wind speed Vw, we may derive the torque produced by the wind on the turbine shaft, as shown in [20]:

$$T_e = \frac{p_w}{\omega_m} = \frac{\frac{1}{2}\rho\pi R^2 C_p v_w^3}{\omega_m} \tag{4}$$

Coefficient The power coefficient of the blade, C_P, is calculated as follows:

$$\begin{aligned} C_P &= K_1\left(\frac{K_2}{\lambda_i} - K_3\beta - K_4\beta^{K_5} - K_6\right)\left(e^{\frac{k_7}{\lambda_i}}\right) \\ \lambda_i &= \frac{1}{\lambda + k_8} \end{aligned} \tag{5}$$

Where λ_i $(i = 1, 2, \ldots\ldots, 8)$ are constant and the tip step ratio (λ_i) and the pitch angle (β).

Another definition for λ_i, the wind speed tip-speed ratio, is as follows:

$$\lambda_i = \frac{\omega_m R}{V_W} \tag{6}$$

The link between wind speed and generator speed, power, and torque may be shown in Tabel I. These numbers were derived as unit values based on $P_{base} = 2$ Mw, N = 1500 rpm, and T_{base} = 12732 Nm.

TABLE I.
RELATION BETWEEN WIND SPEED WITH GENERATOR SPEED, POWER, AND TORQUE

v_w(m/s)	5	6	7	8	9	10	11
ω_m	0.39	0.47	0.55	0.63	0.71	0.79	0.87
p_m	0.08	0.12	0.16	0.21	0.27	0.34	0.41
T_m	0.21	0.26	0.30	0.34	0.39	0.43	0.47
v_w(m/s)	12	13	14	15	16	17	
ω_m	0.94	1.02	1.10	1.18	1.26	1.34	
p_m	0.49	0.58	0.67	0.77	0.87	0.99	
T_m	0.51	0.56	0.60	0.65	0.69	0.73	

4) Methods for Regulating DFIG Converters

Usually, the Rotor Side Converter (RSC) controls the electric torque (or the rotor speed) of the DFIG and the power factor at the stator terminals. The vector technique typically employs a qd rotating frame synchronized with the vector stator flux to regulate rotor currents. In this reference frame, the electric torque is directly proportional to the rotor current along the q-axis.

Also, reactive power regulation in the machine is made by adjusting the d-axis component of the rotor current. Regulating the DC-link voltage and allowing actual power to pass through the converter are the major objectives of the GSC. According to [21], the Vector Controller (VC) approach is often used for the Grid Side Converter (GSC), where the reference frame is aligned with the grid-voltage vector. Controllers for both RSC and GSC are modeled. Fig. 2 presents the MPPT curve, which shows the connection between wind power and wind speed. However, the DFIG can maintain a nearly constant rotational speed when the wind speed is relatively low. So, when the wind speed is high enough, the MPPT torque reference will be higher than the turbine rated torque, and the DFIG will start running at maximum constant torque [22].

It is the job of the GSC and RSC to regulate the DFIG such that, in a steady state, it follows the MPPT curve. The two controllers block schematics are seen in Fig. 3. The GSC controller regulates both the induction generator's terminal voltage (V_s) and the DC-link voltage (V_{DC}). The RSC controller controls the stator reactive power (Q_s) and electric torque (T_e). To operate on the maximum power point tracking (MPPT) curve at a steady state, electric torque (T_e) must be equal to wind torque (T_w) while considering just power losses. So, using the value of T_e^* derived from the MPPT curve shown in Fig. 2, we can get the reference torque, T_e^*. Reactive power control objectives, such as fixed reactive power or unity power factor, determine the value of reference reactive power Q_s [23]. This article chooses the second approach and uses a value of 0 for Q_s^*.

5) Model of The Shaft System

The reliability of power systems is often studied using a two-mass drive train model. The first mass stands for the low speed of the wind turbine shaft, while the second mass refers to the high rate of the DFIG shaft. The state-space representation of

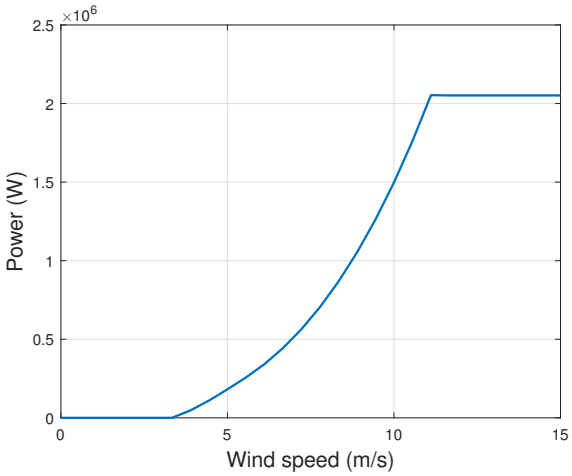

Fig. 2. Wind power and wind speed relationship for MPPT curve.

a system with two masses appears to be this [23]:

$$\frac{d}{dt}\begin{bmatrix}\omega_w\\ \omega_g\\ T_I\end{bmatrix}=\begin{bmatrix}\frac{-2\,B_w-B_g}{2H_w} & \frac{B_w+B_g}{2H_w} & \frac{-1}{2H_w}\\ \frac{B_w+B_g}{2H_g} & \frac{-2\,B_g-B_w}{2H_g} & \frac{1}{2H_g}\\ k_{tg}\omega_e & -k_{tg}\omega_e & 0\end{bmatrix}\begin{bmatrix}\omega_w\\ \omega_g\\ T_I\end{bmatrix}+\begin{bmatrix}\frac{1}{2H_w} & 0 & 0\\ 0 & \frac{1}{2H_g} & 0\\ 0 & 0 & 1\end{bmatrix}\begin{bmatrix}T_{mec}\\ T_e\\ 0\end{bmatrix} \tag{7}$$

Where the inputs for the model of the shaft system are set up T_{mec} and T_e. State variables, on the other hand, are ω_w, ω_g and T_I. Two-mass model constants are B_w, B_g, H_w, H_g, k_{tg}, and ω_e. Each of the parameters is represented in terms of per unit. The ideal wind turbine torque, T_m, may be obtained by consulting Table I for any given wind speed; the value of T_e, on the other hand, can be expressed in terms of the currents of DFIG as follows:

$$T_e = X_m(i_{d_r}i_{q_s}+i_{d_r}i_{q_r}-i_{d_s}i_{q_r}-i_{q_r}i_{d_r}) \tag{8}$$

6) Model of Transmission Line

In power system studies, the dynamics of transmission networks are often disregarded, yet they have a connection to the SSR phenomenon. The transmission line may thus be modeled as a series RLC circuit as shown in Fig 4. The equations of dynamics for each phase are described as follows:

$$R_{line}i_L+L_{line}\frac{di_L}{dt}+v_c=v_s-E_b$$
$$C_{comp}\frac{dv_c}{dt}=i_L \tag{9}$$

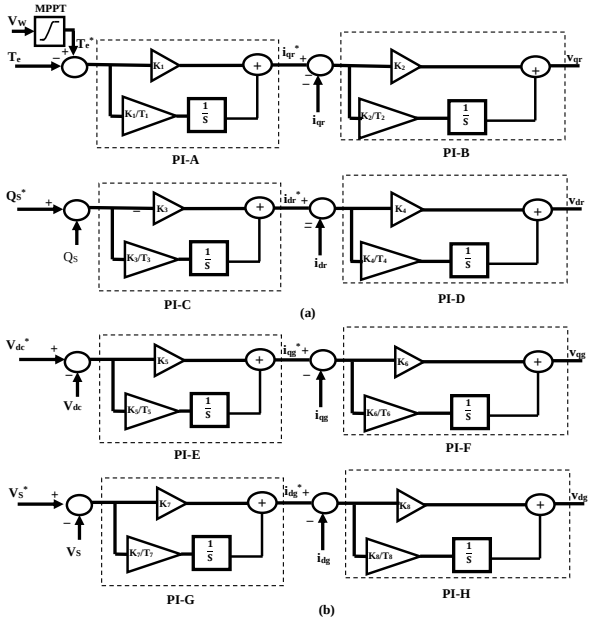

Fig. 3. (a) Rotor side controller. (b) Grid side controller. Rotor and grid side controllers.

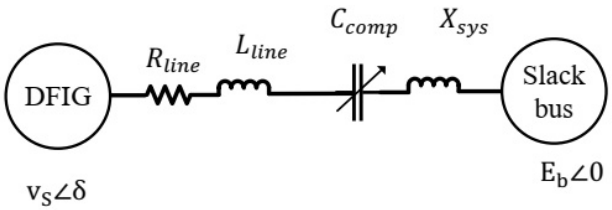

Fig. 4. Transmission line and capacitor compensation model.

By using a state-space model, the equations describing the dynamics of transmission lines may be written as follows:

$$\frac{d}{dt}\begin{bmatrix}i_{qL}\\ i_{dL}\\ v_{qC}\\ v_{dC}\end{bmatrix}=\begin{bmatrix}\frac{-R_{line}}{X_{line}} & -\omega_e & \frac{-1}{X_{line}} & 0\\ \omega_e & \frac{-R_{line}}{X_{line}} & 0 & \frac{-1}{X_{line}}\\ X_{comp} & 0 & 0 & -\omega_e\\ 0 & X_{comp} & \omega_e & 0\end{bmatrix}\begin{bmatrix}i_{qL}\\ i_{dL}\\ v_{qC}\\ v_{dC}\end{bmatrix}+\begin{bmatrix}\omega_b & 0 & 0 & 0\\ 0 & \omega_b & 0 & 0\\ 0 & 0 & 1 & 0\\ 0 & 0 & 0 & 1\end{bmatrix}\begin{bmatrix}\frac{v_{qs}-E_{qb}}{X_{line}}\\ \frac{v_{ds}-E_{db}}{X_{line}}\\ 0\\ 0\end{bmatrix} \tag{10}$$

7) Model of DFIG

The DFIG with the rotor-side converter uses a dynamic model of the sixth order. The model is shown to be [24]

$$\frac{dX_{DFIG}}{dt} = A_{DFIG}X_{DFIG} + B_{DFIG}U_{DFIG} \tag{11}$$

where

$$X_{DFIG}{}^{T} = \begin{bmatrix} i_{q_s} & i_{d_s} & i_{o_s} & i_{q_r} & i_{d_r} & i_{o_r} \end{bmatrix}$$

$$U_{DFIG}{}^{T} = \begin{bmatrix} v_{q_s} & v_{d_s} & v_{o_s} & v_{q_r} & v_{d_r} & v_{o_r} \end{bmatrix}$$

$$B_{DFIG} = \omega_b \begin{bmatrix} X_s & 0 & 0 & X_m & 0 & 0 \\ 0 & X_s & 0 & 0 & X_m & 0 \\ 0 & 0 & X_{ls} & 0 & 0 & 0 \\ X_m & 0 & 0 & X_R & 0 & 0 \\ 0 & X_m & 0 & 0 & X_R & 0 \\ 0 & 0 & 0 & 0 & 0 & X_{l_R} \end{bmatrix}$$

$$A_{DFIG} = -B_{DFIG} \begin{bmatrix} r_s & aX_s & 0 & 0 & aX_m & 0 \\ -aX_s & r_s & 0 & -aX_m & 0 & 0 \\ 0 & 0 & r_s & 0 & 0 & 0 \\ 0 & bX_m & 0 & r_R & bX_R & 0 \\ -bX_m & 0 & 0 & -bX_R & r_R & 0 \\ 0 & 0 & 0 & 0 & 0 & r_R \end{bmatrix}$$

$$a = \frac{\omega_s}{\omega_b}$$

$$b = \frac{\omega_s - \omega_s}{\omega_b}$$

The values of the constants (electrical parameters) in appendix are represented by B_{DFIG}, the inputs by U_{DFIG}, the state variables by X_{DFIG}, and A_{DFIG} by a constant and a single variable (rotor speed ω_r). Direct, quadrature, and zero-sequence components are indicated by d, q, and 0 on the stator and rotor sides, respectively. The parameters i_{0s}, i_{0r}, v_{0s}, and v_{0r} are all equal to zero, indicating that the system is in balance.

8) Model DC-LINK

In this research, they analyze the behavior of DC-link capacitors. Fig. 1 depicts the DC-link separated back-to-back converters connecting the DFIG to the grid. The DC-link is developed as a first-order model to consider capacitor dynamics in the DC-link.

$$C_{link}v_{link}\frac{v_{link}}{dt} = P_{rotor} - P_{grid} \tag{12}$$

Both the rotor-side converter's active power, P_r, and the grid-side converter's active power, P_g, are calculated as:

$$P_r = (\frac{1}{2})(v_{qr}i_{qr} + v_{dr}i_{dr}) \tag{13}$$

$$P_g = (\frac{1}{2})(v_{qg}i_{qg} + v_{dg}i_{dg}) \tag{14}$$

9) Model for an Integrated System

Certain more algebraic equations are needed to combine the DFIG model with the transmission line model.

First, the current through the GSC is determined by applying KCL at the intersection of the stator, GSC, and transmission line (see Fig. 1). As a result, they may derive the following equation:

$$i_{grid} = i_{stator} + i_{line} \tag{15}$$

Currents in the GSC along the qd axis may be expressed as

$$i_{qg} = i_{qs} + i_{qL} \tag{16}$$

$$i_{dg} = i_{ds} + i_{dL} \tag{17}$$

Second, to determine the DFIG terminal voltage, KVL is applied at an identical position.

$$v_{grid} - v_{stator} = jX_{gc}i_{grid} \tag{18}$$

where v_{grid} is being supplied by the GSC controllers. The voltages at the terminals of the qd-axis are given as:

$$v_{qs} = v_{qg} - jX_{gc}i_{grid} \tag{19}$$

$$v_{ds} = v_{dg} + jX_{gc}i_{grid} \tag{20}$$

The reactive power of the stator is calculated as

$$Q_s = (\frac{1}{2})(v_{qs}i_{ds} - v_{ds}i_{qs}) \tag{21}$$

III. Initial Values of State Variables Calculation

The primary objective of this process is to determine the values of the initial state vector X_0 when the operating point is altered (by modifying the compensation level, $K = \frac{X_c}{X_L}$, and wind speed). Accordingly, the initial value may be defined as follows.

$$x_0 = \begin{bmatrix} \omega_w & \omega_g & T_l & i_{qL} & i_{dL} & v_{qc} & v_{dc} & i_{qs} \\ i_{ds} & i_{qr} & i_{dr} & v_{link} & & & & \end{bmatrix} \tag{22}$$

Anywhere in the operational range, the initial V_{DC} voltage is 1200 V. Based on the wind speed, the initial values for the shaft system (ω_w, ω_g,and T_l) may be found in Table I The

remaining initial values may be calculated in three stages. Step 1 entails doing a load flow analysis. In stages 2 and 3, they acquire the starting values for the transmission line and DFIG.

step 1: The Analysis of Load Flow

The steady-state equivalent circuit of the system is seen in Fig. 3; the system is comprised of two buses, denoted as PV and infinite. Voltage magnitude and active power are planned for the generator bus (1), DFIG stator node as if it were a PV bus. Since we already know the magnitude and phase angle of the voltage on the infinite bus (2), we may consider it a slack bus. The following is the load flow study performed to achieve the angle δ_1 at the PV bus [14]

$$\frac{\mathrm{R_{line}\, v_s^2}}{\mathrm{R_{line}^2 + \left(x_{line} + x_{sys} - x_{comp}\right)^2}} - \frac{\mathrm{R_{line}\, v_s E_b}}{\mathrm{{R_{line}}^2 + \left(x_{line} + x_{sys} - x_{comp}\right)^2}} \cos(\delta_1) + \frac{\mathrm{R_{line}\, v_s \left(x_{line} + x_{sys} - x_{comp}\right)}}{\mathrm{{R_{line}}^2 + \left(x_{line} + x_{sys} - x_{comp}\right)^2}} \sin(\delta_1) - \mathrm{P_m} = 0 \tag{23}$$

All other parameters remain unchanged when X_{comp} and P_m depend on the operating point. In the preceding equation, X_{line} represents the sum of the reactance of the transmission line X_L (0.5 p.u) and the transformer X_T (0.14 p.u). As an example, assume a compensation level of 20 per cent (X_{comp}= 0.1 p.u) and a wind speed of 15 m/s (P_m =0.7727 per unit). With the aforementioned formula, δ_1 equals 0.4784 radians.

step 2: Transmission line initial conditions (i_{qL}, i_{dL}, v_{qc}, and v_{dc})

As seen in Fig. 5 , the q-axis of the synchronously rotating qd frame often coincides with the stator voltage of DFIG versus. Quadrature and direct-axis voltage components for a DFIG stator are written as:

$$\begin{aligned} v_{qs} &= v_s = E_b = 1 per\ unit \\ v_{ds} &= 0 \end{aligned} \tag{24}$$

The direct and quadrature axes of the infinite bus voltage components are computed as:

$$\begin{aligned} E_{db} &= E_b \sin(\delta_1) \\ E_{qb} &= E_b \cos(\delta_1) \end{aligned} \tag{25}$$

The transmission line model requires four equations due to four state variables. The last four transmission line equations are obtained when the time derivatives of (10) are adjusted to zero.

$$\begin{aligned} &-\frac{R_{line}}{X_{line}} i_{qL} - \omega_e i_{dL} - \frac{1}{X_{line}} v_{qc} + \frac{v_{qs} - E_b \cos(\delta_1)}{X_{line}} = 0 \\ &\omega_e i_{qL} - \frac{R_{line}}{X_{line}} i_{dc} - \frac{1}{X_{line}} v_{dc} + \frac{v_{ds} - E_b \cos(\delta_1)}{X_{line}} = 0 \\ &X_{comp} i_{qL} - \omega_e v_{dc} = 0 \\ &X_{comp} i_{dL} - \omega_e v_{qc} = 0 \end{aligned} \tag{26}$$

The result of (24) It is possible to determine the starting values for i_{qL}, i_{dL}, v_{qc}, and v_{dc}. As an example, assuming a wind speed of 15 m/s and a correction level of 20 per cent, 0.4784 is rad. This results in the values $i_{qL0} = 0.8590$, $i_{dL0} = 0.1761$, $v_{qc0} = 0.0176$, and $v_{dc0} = 00859 p.u.$

step 3: Variables of the DFIG state (i_{qs}, i_{ds}, i_{qr}, and i_{dr}) and their initial values.

The stator and rotor currents of a DFIG may be calculated using the i_{qL} and i_{dL} currents in the transmission lines. From (24) and (25), they can derive the rotor currents i_{dr} and i_{qr}; from (26) and (27), they can get the rotor voltages $v_{dr}$and v_{qr}; from (28), they can get the quadrature axis of the DFIG grid side converter current iqg; and from (29) and (30), they can get the stator currents [17].

$$i_{dr} = a_1 i_{qg} + b_1 \tag{27}$$

$$i_{qr} = a_2 i_{qg} + b_2 \tag{28}$$

$$v_{qr} = a_3 i_{qg} + b_3 \tag{29}$$

$$v_{dr} = a_4 i_{qg} + b_4 \tag{30}$$

where

$$\mathrm{a_1} = \left(\frac{\omega_b \mathrm{r_S}}{\omega_e \mathrm{x_m}} + \frac{\mathrm{x_S v_{ds}}}{\mathrm{x_m v_{qs}}} \right)$$

$$b_1 = \left(\frac{Q_{\mathrm{gref}} X_s}{X_m v_{qs}} - \frac{\omega_b}{\omega_e X_m} v_{qs} - \frac{\omega_b r_S}{\omega_e X_m} i_{qL} - \frac{X_S}{X_m} i_{dL} \right)$$

$$\mathrm{a_2} = \left(\frac{\mathrm{X_s}}{\mathrm{X_m}} - \frac{\omega_b \mathrm{r_s v_{ds}}}{\omega_e \mathrm{X_m v_{qs}}} \right)$$

$$b_2 = \left(\frac{\omega_b}{\omega_e X_m} v_{ds} - \frac{X_s}{X_m} i_{qL} + \frac{\omega_b r_s}{\omega_e X_m} i_{dL} - \frac{Q_{gref} \omega_b r_s}{\omega_e X_m v_{qs}} \right)$$

$$\mathrm{a_3} = \left(\frac{(\omega_e - \omega_r)\mathrm{X_m}}{\omega_b} \frac{\mathrm{v_{ds}}}{\mathrm{v_{qs}}} - \mathrm{a_2 r_r} - \frac{(\omega_e - \omega_r)\mathrm{X_r}}{\omega_b} \mathrm{a_1} \right)$$

$$\mathrm{b_3} = \left(\frac{(\omega_e - \omega_r)\mathrm{Q_{gref} X_m}}{\omega_b \mathrm{v_{qs}}} - \frac{(\omega_e - \omega_r)\mathrm{X_m}}{\omega_b} \mathrm{i_{dL}} - \mathrm{b_2 r_r} - \frac{(\omega_e - \omega_r)\mathrm{X_r}}{\omega_b} \mathrm{b_1} \right)$$

$$\mathrm{a_4} = \left(\frac{(\omega_e - \omega_r)\mathrm{X_r a_2}}{\omega_b} - \frac{(\omega_e - \omega_r)\mathrm{X_m}}{\omega_b} - \mathrm{a_2 r_r} \right)$$

$$\mathrm{b_4} = \left(\frac{(\omega_e - \omega_r)\mathrm{X_r b_2}}{\omega_b} - \frac{(\omega_e - \omega_r)\mathrm{X_m}}{\omega_b} \mathrm{i_{qL}} - \mathrm{b_1 r_r} \right)$$

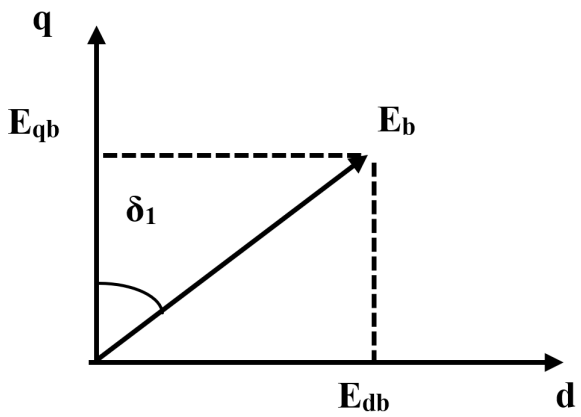

Fig. 5. Infinite bus voltage is represented by a dq frame in DFIG.

TABLE II.
THE INITIAL VALUES OF THE SYSTEM STATE VARIABLES, WITH K = 50 PER CENT AND V_w = 9 M/S

$\omega_{go} = 1.18$	$\omega_{mo} = 1.18$	$T_e = 0.65$	$\delta_1 = 0.4784$
i_{qL0} = 1.3687	i_{dL0} = 0.2497	v_{cq0} = 0.0749	v_{cd0} = 0.4106
i_{qs0} = 1.1695	i_{ds0} = 0.2497	v_{qc0} = 1.2440	v_{dc0} = 0.0889

and

$$a_5 i_{qg}^2 + b_5 i_{qg} c_5 = 0 \tag{31}$$

where

$$a_5 = a_2 a_3 + a_1 a_4$$

$$b_5 = -v_{qs} - \frac{v_{ds}^2}{v_{qs}} + a_3 b_2 + a_2 b_3 + a_4 b_1 + a_1 b_4$$

$$c_5 = (-\frac{Q_{gref} v_{ds}}{v_{qs}} + b_2 b_3 + b_1 b_4)$$

$$i_{qs} = -(i_{qL} - i_{qg}) \tag{32}$$

$$i_{ds} = -(i_{qL} - \frac{v_d s}{v_q s} i_{qg} - \frac{Q_{gref}}{v_q s}) \tag{33}$$

The starting values of the state variables of the system at 60 per cent compensation and 15 m/s wind speed are shown in Table II.

IV. ANALYSIS OF THE SSR METHOD

Using minor perturbations in the states and inputs to numerically compute the partial derivatives [25], *MATLAB/Simulink* can estimate the state-space matrices A, B, C, and D in a linearized approximation. After supplying the starting values for each state in the *Matlab/Simulink* model, and $SSR-DFIG$ is the name that will be used to save the file, the eigenvalues of the system may be calculated with the help of the following MATLAB commands:

$<< [ABCD] = linmod('SSR-DFIG')$

$<< eig(A)$

Table III lists the 22 modes the system may attain given its 22nd state variables. Tables IV and V show the relation be-

TABLE III.
EIGENVALUES OF THE WHOLE SYSTEM'S MODES WHEN THE CORRECTION LEVEL IS SET TO 50 PER CENT , AND THE WIND SPEED IS 9 M/S.

Mode	description	Eignvalue magnitude	Freq.(Hz)
$\lambda_{1,2}$	SSR eigenvalue	-2.1±j166.4	26.4
$\lambda_{3,4}$	Sup-synchronous eigenvalue	20.1±j586.4	93.3
$\lambda_{5,6}$	Torsional eigenvalue	-0.4±j1	0.15
$\lambda_{7,8}$	Electro-mechanical eigenvalue	-52.3±j53.8	8.5
$\lambda_{9,10}$	Very high-frequency eigenvalues	1763±j870.3	138.5
$\lambda_{11,12}$	PI Controllers eigenvalue	-23.2±j43.8	6.97
$\lambda_{13,14}$	PI Controllers eigenvalue	0±j0	0
λ_{15}	No oscillatory eigenvalue	-10	0
λ_{16}	No oscillatory eigenvalue	-8.4	0
λ_{17}	No oscillatory eigenvalue	-5.2	0
λ_{18}	No oscillatory eigenvalue	3.2	0
λ_{19}	No oscillatory eigenvalue	-1.1	0
λ_{20}	No oscillatory eigenvalue	-0.5	0
λ_{21}	No oscillatory eigenvalue	-48.2	0
λ_{22}	No oscillatory eigenvalue	-37.7	0

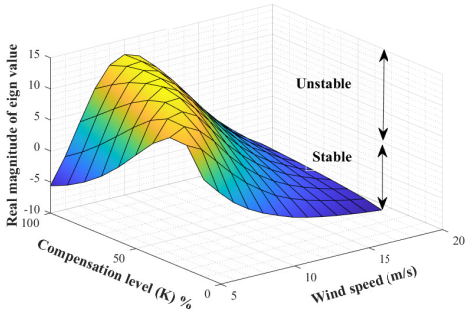

Fig. 6. Relation between wind speed and compensation level for the real eigenvalues.

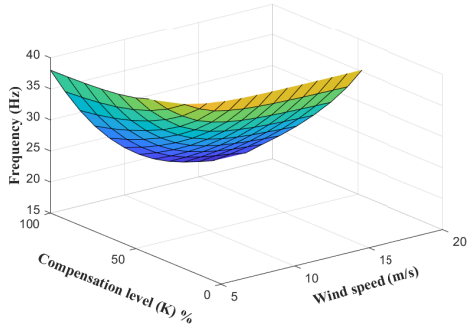

Fig. 7. Relation between wind speed and compensation level for different values of natural frequency.

tween wind speed and compensation level for the real eigenvalues and natural frequency. The results obtained from the tables may be represented graphically in Fig. 6 and Fig. 7, respectively. These figures are relation the real value of eigenvalues with changes in compensation level and wind speed to show the boundary of the region stability system.

V. Using Matlab/Simulink to Calculate The System's Eigenvalues

In this part of the article, an eigenvalue analysis is carried out using both the technique that has been provided and the approach that was iterated to validate the efficiency and precision of the presented method. The findings of the obtained eigenvalue analysis are contrasted with the results of a time-domain simulation, as shown in Fig. 8, carried out with varying amounts of compensation and wind speeds.

1) Different Levels of Compensation

Here, time-domain simulation is used to examine how various compensation schemes affect the system's robustness. Fig. 9 and Fig. 10 is a time-domain simulation demonstrating that raising the compensation level causes the system to become unstable. When comparing the power response at speeds 10 m/s and 15m/s, we note that the stability of the system decreases with increasing the amount of compensation; however, the drop becomes more apparent at speed 10 m/s since the system is in the stage of instability of the power produced by the wind turbine at that speed. They notice that the system is in a state of purification after a period of instability at a rate of 10 m/s, and the compensation value is 100%. Table VI presents the results of examining eigenvalues based on the proposed and non-iterative approaches. The following observations may be derived from Table VI by comparing the results of the FFT analysis with those of the eigenvalue analysis: 1- It is abundantly evident that the acquired frequency using the suggested approach is very close to the frequency obtained using FFT analysis (f_{FFT}= 26.8 Hz, fproposed = 26.769 Hz at 15 m/s wind speed and 60 per cent compensation level). 2- The frequency that can be achieved using the non-iterative technique is lower than the frequency that can be obtained with the FFT (f_{FFT} = 26.8 Hz, fnon-iterative = 26.467 Hz at 15 m/s wind speed and 60 per cent compensation level). 3- At any given compensation level, the accuracy of the suggested technique exceeds that of the non-iterative method. For instance, the error based on the presented approach is around 0.115 percent, but an error based on the method that was non-iterative is approximately 1.24 percent at 15 m/s wind speed and 60 per cent compensation level.

2) Several Winds Speed

Using time-domain simulation and eigenvalue analysis based on the suggested technique, this paper looks at the impact of varying wind speeds on the system's stability. As seen in Fig. 11 and Fig. 12, the system becomes stable when the wind speed increases for two compensation levels 50% and 10%. Table VII displays the results of an eigenvalue analysis using both the proposed and the non-iterative methods. This table shows the following conclusion: 1- The frequency acquired using the suggested approach is quite close to that obtained using FFT analysis (f_{FFT} = 34.6 Hz, $f_{proposed}$ = 34.593 Hz at 7 m/s wind speed and 50 per cent compensation level). 2- The non-iterative approach yields an inaccurate frequency estimate where the error percentage at 7 m/s wind speed and 50 per cent compensation level is equal to 0.144 at the non-iterative method while equal to 0.02 at the proposed method. 3- At every wind speed, the results obtained using the proposed approach are superior to those obtained using the non-iterative method.

TABLE IV.
WIND SPEED AND COMPENSATION LEVEL FOR THE REAL EIGENVALUES.

k\ V_W	5	6	7	8	9	10	11	12	13	14	15	16	17
10	5.662	3.102	0.850	-0.787	-2.039	-3.005	-3.871	-4.466	-4.950	-5.349	-5.685	-5.973	-6.224
20	10.05	8.822	6.330	3.865	1.702	-0.008	-1.537	-2.588	-3.428	-4.111	-4.677	-5.155	-5.566
30	10.17	11.33	10.10	7.813	4.914	2.543	0.627	-0.892	-2.102	-3.077	-3.859	-4.544	-5.113
40	8.060	11.47	12.02	10.74	7.909	5.045	2.721	0.779	-0.816	-2.100	-3.091	-4.010	-4.745
50	5.033	10.05	12.39	12.50	10.30	7.579	4.862	2.461	0.479	-1.126	-2.316	-3.510	-4.423
60	1.984	7.775	11.58	13.15	11.93	9.652	6.848	4.140	1.797	-0.136	-1.500	-3.025	-4.134
70	-0.628	5.163	9.973	12.54	12.78	11.21	8.621	5.767	3.123	0.869	-0.999	-2.554	-3.874
80	-2.713	2.629	7.906	11.54	12.91	12.21	10.08	7.275	4.425	1.877	-0.484	-2.109	-3.636
90	-4.358	0.386	5.674	10.04	12.42	12.66	11.15	8.585	5.649	2.853	0.392	-1.720	-5.655
100	-5.607	-1.498	3.501	8.242	11.45	12.59	11.80	9.620	6.726	3.731	0.969	-1.442	-5.759

TABLE V.
WIND SPEED AND COMPENSATION LEVEL FOR DIFFERENT VALUES OF NATURAL FREQUENCY.

k\ V_W	5	6	7	8	9	10	11	12	13	14	15	16	17
10	47.47	46.93	46.66	46.50	46.42	46.39	46.37	46.36	46.35	46.34	46.34	46.34	46.34
20	43.82	42.60	41.81	41.31	41.05	40.91	40.84	40.78	40.74	40.71	40.69	40.68	40.67
30	41.63	39.90	38.62	37.71	37.21	36.88	36.69	36.56	36.48	36.42	36.38	36.35	36.32
40	40.20	38.02	36.33	35.01	34.19	33.63	33.28	33.08	32.93	32.83	32.77	32.71	32.66
50	39.27	36.64	34.59	32.91	31.79	30.96	30.42	30.08	29.86	29.70	29.60	29.51	29.44
60	38.71	35.65	33.24	31.24	29.82	28.72	27.96	27.46	27.13	26.91	26.76	26.62	26.52
70	38.39	34.96	32.19	29.97	28.19	26.82	25.83	25.14	24.68	24.37	24.15	23.98	23.84
80	38.20	34.49	31.38	28.86	26.83	25.21	23.97	23.08	22.47	22.05	21.71	21.53	21.32
90	38.08	34.18	30.78	27.97	25.68	23.82	22.35	21.25	20.47	19.92	19.52	19.21	18.76
100	38.01	33.97	30.34	27.26	24.71	22.62	20.93	19.61	18.63	17.93	17.41	16.99	18.95

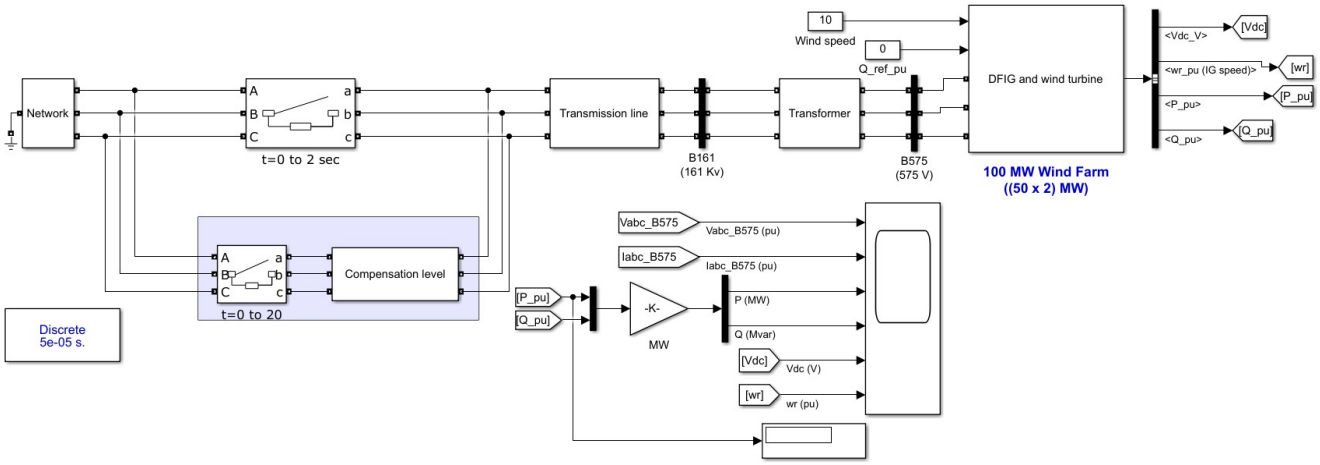

Fig. 8. All-system simulation model.

VI. CONCLUSION

A established analytical technique for establishing the beginning values for SSR analysis may be found in this work, done recently. The analytical technique does away with the necessity of making assumptions; in addition to this, it is precise, uncomplicated, simple, easy to put into practice, computationally efficient, and time-efficient. The extraction of the

TABLE VI.
FREQUENCY ANALYSIS (f_{FFT}) OF THE ELECTRICAL POWER SIGNAL (P), EIGENVALUE ANALYSIS (NON-ITERATIVE APPROACH), AND EIGENVALUE ANALYSIS (PROPOSED METHOD) AT VARYING DEGREES OF CORRECTION.

V_{wax}	K%	f_{EET}	Non-iterative method [17]	Freq.	Error %	Present method	Freq.	Error %
15	20	40.7	$-4.43 \pm j251.3$	39.995	1.73	$-4.67 \pm j255.7$	40.69	0.02
	40	32.8	$-2.99 \pm j202.3$	32.197	1.8	$-3.09 \pm j205.91$	32.773	0.082
	60	26.8	$-1.32 \pm j166.3$	26.467	1.24	$-1.5 \pm j168.2$	26.769	0.115
	80	21.9	$-0.423 \pm j134.9$	21.47	1.96	$-0.484 \pm j136.466$	21.719	0.826
	100	17.5	$0.924 \pm j108.99$	17.346	0.88	$0.9694 \pm j109.446$	17.4189	0.463
10	20	41	$-0.0078 \pm j236.54$	37.646	8.1	$-0.00847 \pm j237.046$	40.9101	0.219
	40	33.7	$5.014 \pm j210.8$	33.549	0.44	$5.045 \pm j211.35$	33.637	0.186
	60	28.8	$9.322 \pm j180.08$	28.66	0.486	$9.652 \pm j180.479$	28.724	0.263
	80	25.3	$12.04 \pm j158.04$	25.152	0.584	$12.216 \pm j158.401$	25.210	0.355
	100	22.7	$12.325 \pm j141.98$	22.596	0.4581	$12.595 \pm j142.128$	22.62	0.352

TABLE VII.
CALCULATE THE FREQUENCY CONTENT OF THE ELECTRICAL POWER SIGNAL (P) USING FAST FOURIER TRANSFORM (f_{FFT}), NON-ITERATIVE EIGENVALUE ANALYSIS, AND THE PROPOSED EIGENVALUE ANALYSIS AT VARIABLE WIND SPEEDS.

K%	V_{wx}	f_{FET}	Non-iterative method [17]	Freq.	Error %	Present method	Freq.	Error %
50	5	39.4	$4.98 \pm j244.32$	38.88	1.31	$5.03 \pm j246.795$	39.278	0.309
	7	34.6	$11.98 \pm j217.1$	34.55	0.144	$12.027 \pm j217.359$	34.593	0.02
	9	31.85	$10.12 \pm j199.21$	31.705	0.455	$10.3 \pm j199.749$	31.791	0.185
	11	30.6	$4.802 \pm j190.98$	30.395	0.669	$4.862 \pm j191.196$	30.429	0.558
	13	29.9	$0.442 \pm j185.2$	29.475	1.421	$0.479 \pm j187.622$	29.8609	0.1307
	15	29.75	$-2.142 \pm j184.3$	29.33	1.41	$-2.316 \pm j186.041$	29.609	0.4739
10	5	47.6	$5.521 \pm j297.91$	47.413	0.39	$5.66 \pm j298.321$	47.479	0.254
	7	46.8	$0.792 \pm j290.3$	46.202	1.27	$0.8507 \pm j293.17$	46.66	0.2991
	9	46.5	$-1.986 \pm j290.42$	46.22	0.6021	$-2.039 \pm j291.727$	46.429	0.152
	11	46.45	$-3.351 \pm j290.02$	46.158	0.628	$-3.871 \pm j291.405$	46.378	0.155
	13	46.38	$-4.42 \pm j289.85$	46.131	0.536	$-4.95 \pm j291.246$	46.353	0.0582
	15	46.36	$-5.423 \pm j289.45$	46.067	0.632	$-5.685 \pm j291.183$	46.343	0.0366

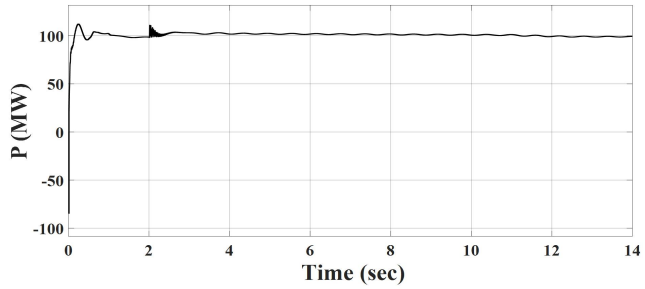

(a) $v_w = 15m/s,\ K = 20$ *per cent*

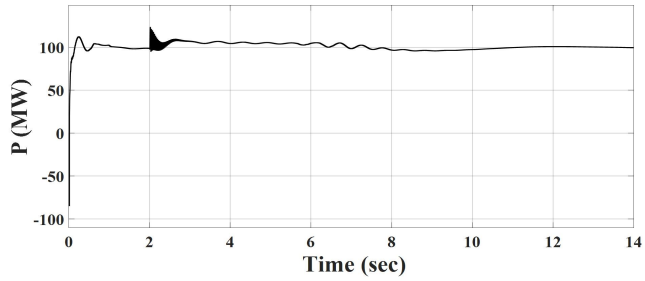

(b) $v_w = 15m/s,\ K = 40$ *per cent*

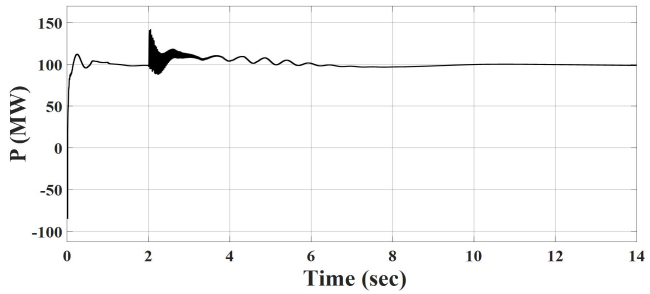

(c) $v_w = 15m/s,\ K = 60$ *per cent*

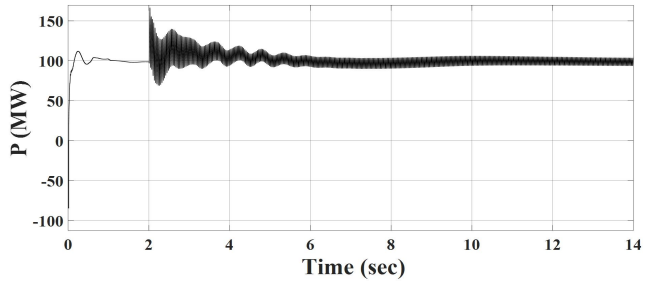

(d) $v_w = 15m/s,\ K = 80$ *per cent*

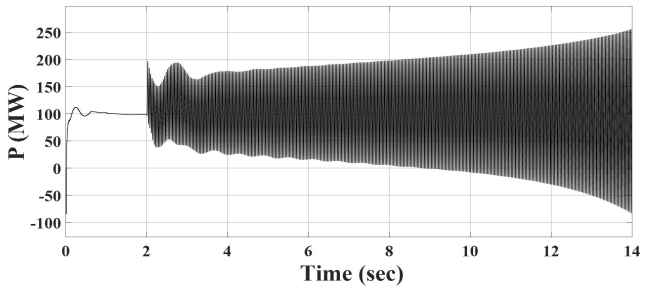

(e) $v_w = 15m/s,\ K = 100$ *per cent*

Fig. 9. Response of electrical power to changes in compensation level for 15 m/s wind speed.

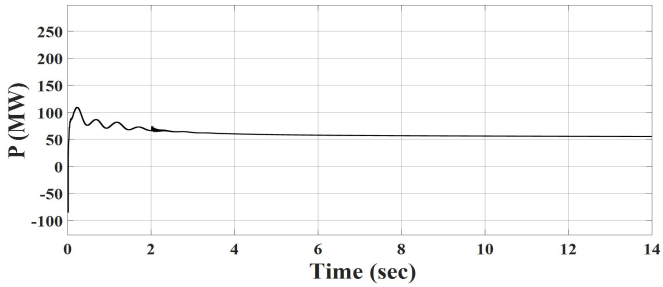

(a) $v_w = 10m/s,\ K = 20$ *per cent*

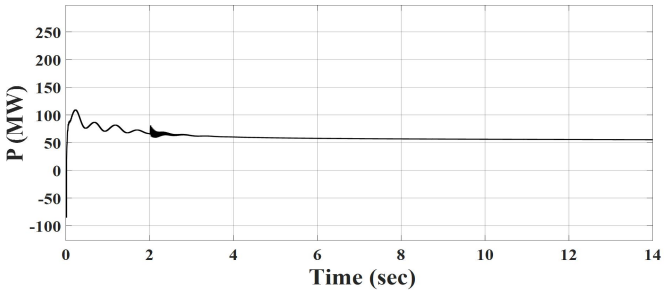

(b) $v_w = 10m/s,\ K = 40$ *per cent*

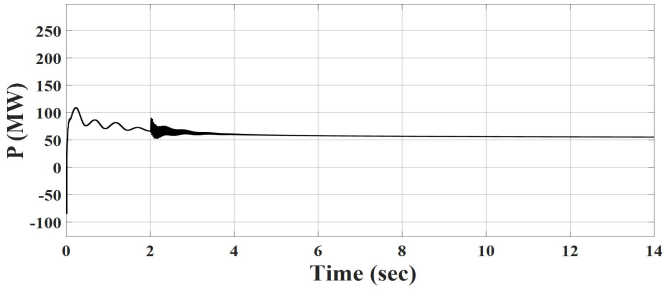

(c) $v_w = 10m/s,\ K = 60$ *per cent*

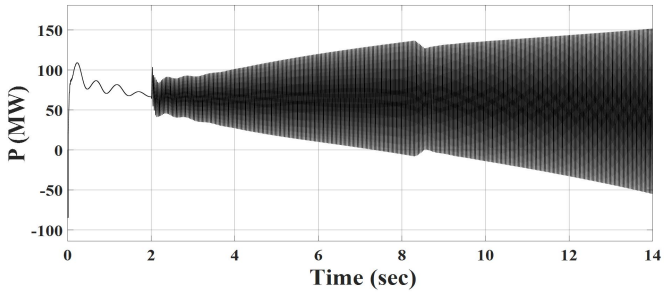

(d) $v_w = 10m/s,\ K = 80$ *per cent*

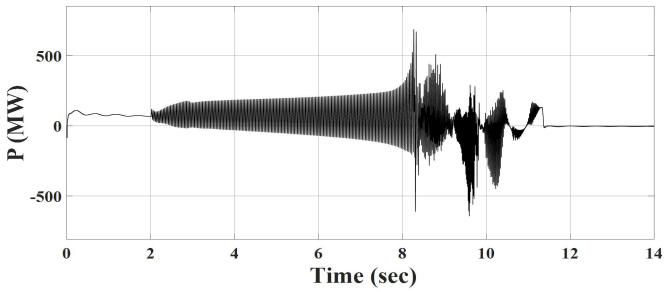

(e) $v_w = 10m/s,\ K = 100$ *per cent*

Fig. 10. Response of electrical power to changes in compensation level for 10 m/s wind speed.

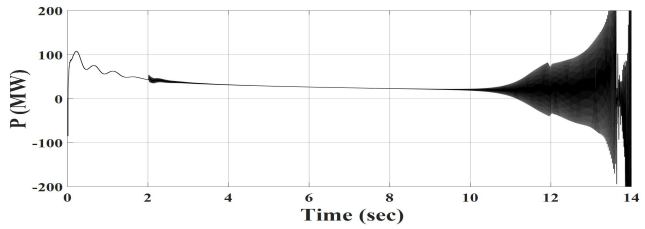

(a) $v_w = 5m/s,\ K = 50\ per\ cent$

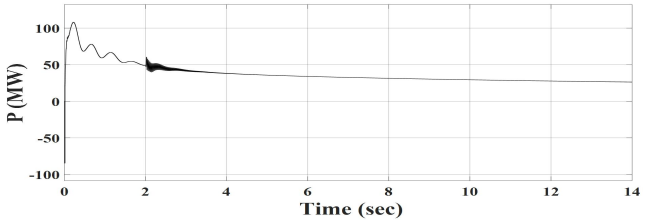

(b) $v_w = 7m/s,\ K = 50\ per\ cent$

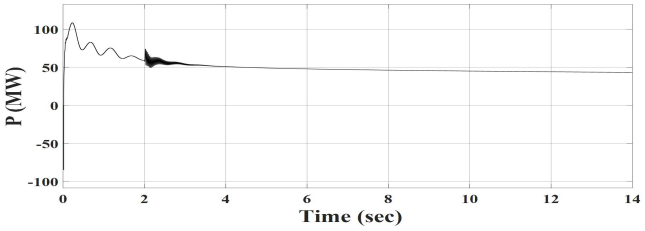

(c) $v_w = 9m/s,\ K = 50\ per\ cent$

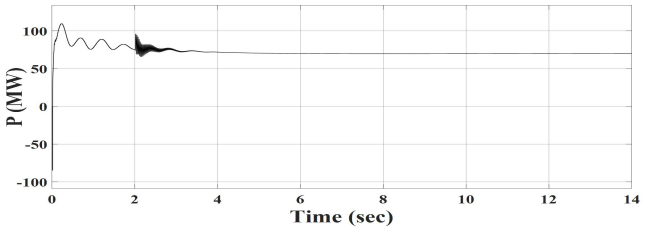

(d) $v_w = 11m/s,\ K = 50\ per\ cent$

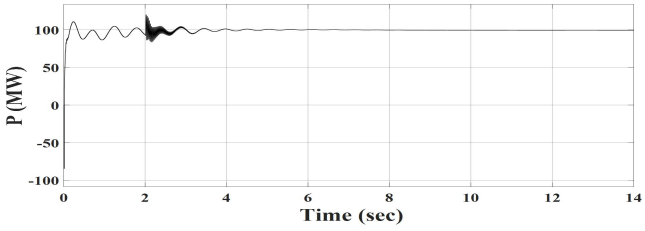

(e) $v_w = 13m/s,\ K = 50\ per\ cent$

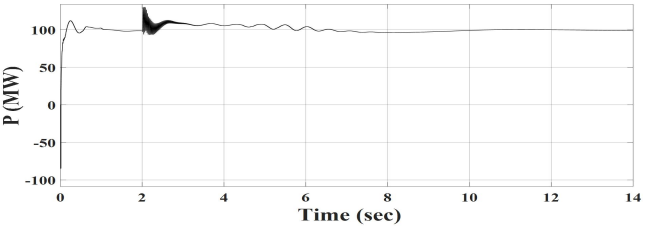

(f) $v_w = 15m/s,\ K = 50\ per\ cent$

Fig. 11. Response of electrical power to changes in wind speed for 50 per cent value of compensation level.

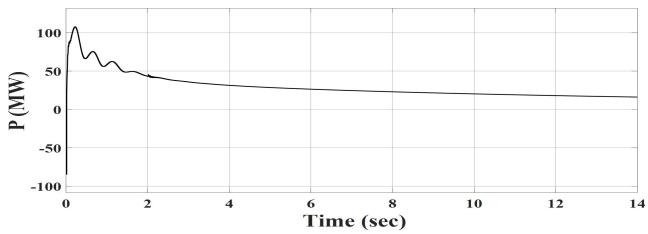

(a) $v_w = 5m/s,\ K = 10\ per\ cent$

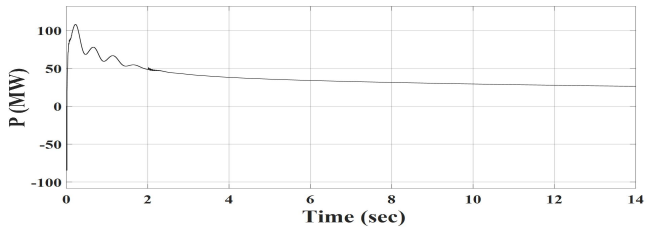

(b) $v_w = 7m/s,\ K = 10\ per\ cent$

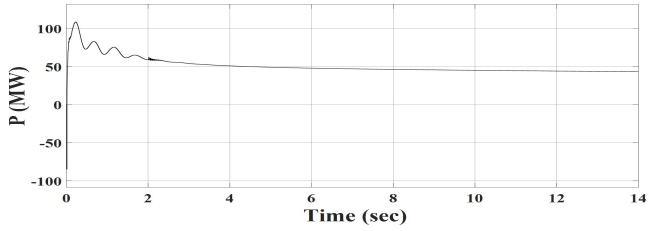

(c) $v_w = 9m/s,\ K = 10\ per\ cent$

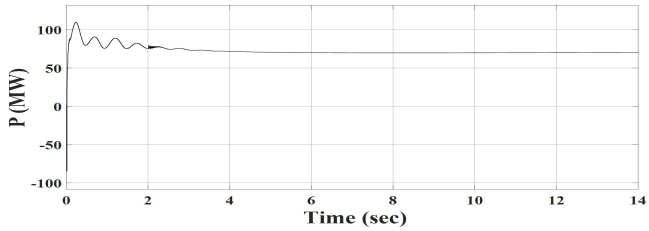

(d) $v_w = 11m/s,\ K = 10\ per\ cent$

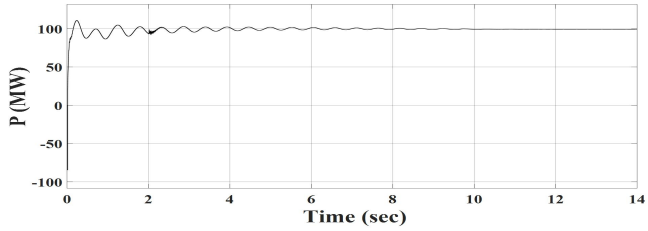

(e) $v_w = 13m/s,\quad K = 10\ per\ cent$

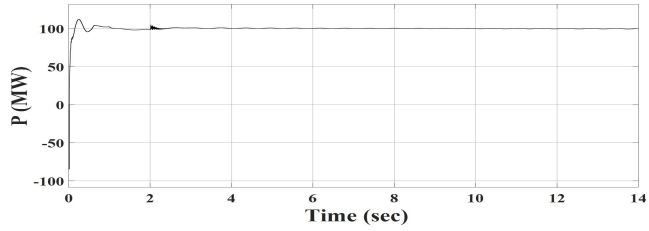

(f) $v_w = 15m/s,\quad K = 10\ per\ cent$

Fig. 12. Response of electrical power to changes in wind speed for 10 per cent value of compensation level.

eigenvalues and the computation of the DFIG steady-state operating point have been provided. The findings of the eigenvalue for the recommended approach and the non-iterative approach were compared with the simulation results at various degrees of correction and with varying wind speeds. The fact that the time-domain simulation matches the eigenvalue analysis based on the suggested strategy demonstrates its superiority and accuracy compared to the non-iterative method across all situations examined. In the study context, it has been observed that raising compensation levels with a decrease in wind speed results in system instability. Consequently, adjusting the compensation level based on the prevailing wind speed is recommended.

Conflict of Interest

The authors have no conflict of relevant interest to this article.

References

[1] H. A. Mohammadpour and E. Santi, "Sub-synchronous resonance analysis in dfig-based wind farms: Definitions and problem identification — part i," *2014 IEEE Energy Conversion Congress and Exposition (ECCE)*, pp. 812–819, 2014.

[2] K. Padiyar, *Analysis of subsynchronous resonance in power systems*. Springer Science & Business Media, 2012.

[3] Y. Liu, J. Zheng, Q. Chen, Z. Duan, Y. Tian, M. Ban, and Z. Li, "Mmc-statcom supplementary wide-band damping control to mitigate subsynchronous control interaction in wind farms," *International Journal of Electrical Power & Energy Systems*, vol. 141, p. 108171, 2022.

[4] M. Ghafouri, U. Karaagac, J. Mahseredjian, and H. Karimi, "Ssci damping controller design for series-compensated dfig-based wind parks considering implementation challenges," *IEEE Transactions on Power Systems*, vol. 34, no. 4, pp. 2644–2653, 2019.

[5] J. Yao, X. Wang, J. Li, R. Liu, and H. Zhang, "Sub-synchronous resonance damping control for series-compensated dfig-based wind farm with improved particle swarm optimization algorithm," *IEEE Transactions on Energy Conversion*, vol. 34, no. 2, pp. 849–859, 2018.

[6] L. Wang, X. Xie, Q. Jiang, H. Liu, Y. Li, and H. Liu, "Investigation of ssr in practical dfig-based wind farms connected to a series-compensated power system," *IEEE Transactions on Power Systems*, vol. 30, no. 5, pp. 2772–2779, 2014.

[7] X. Xie, X. Zhang, H. Liu, H. Liu, Y. Li, and C. Zhang, "Characteristic analysis of subsynchronous resonance in practical wind farms connected to series-compensated transmissions," *IEEE Transactions on Energy Conversion*, vol. 32, no. 3, pp. 1117–1126, 2017.

[8] P. Li, L. Xiong, F. Wu, M. Ma, and J. Wang, "Sliding mode controller based on feedback linearization for damping of sub-synchronous control interaction in dfig-based wind power plants," *International Journal of Electrical Power & Energy Systems*, vol. 107, pp. 239–250, 2019.

[9] H. A. Mohammadpour and E. Santi, "Modeling and control of gate-controlled series capacitor interfaced with a dfig-based wind farm," *IEEE Transactions on Industrial Electronics*, vol. 62, no. 2, pp. 1022–1033, 2014.

[10] S. O. Faried, I. Unal, D. Rai, and J. Mahseredjian, "Utilizing dfig-based wind farms for damping subsynchronous resonance in nearby turbine-generators," *IEEE Transactions on Power Systems*, vol. 28, no. 1, pp. 452–459, 2012.

[11] P.-H. Huang, M. S. El Moursi, W. Xiao, and J. L. Kirtley, "Subsynchronous resonance mitigation for series-compensated dfig-based wind farm by using two-degree-of-freedom control strategy," *IEEE Transactions on Power Systems*, vol. 30, no. 3, pp. 1442–1454, 2014.

[12] A. E. Leon and J. A. Solsona, "Sub-synchronous interaction damping control for dfig wind turbines," *IEEE Transactions on Power Systems*, vol. 30, no. 1, pp. 419–428, 2014.

[13] H. A. Mohammadpour, A. Ghaderi, and E. Santi, "Analysis of sub-synchronous resonance in doubly-fed induction generator-based wind farms interfaced with gate–controlled series capacitor," *IET Generation, Transmission & Distribution*, vol. 8, no. 12, pp. 1998–2011, 2014.

[14] H. A. Mohammadpour and E. Santi, *Analysis of sub-synchronous resonance (SSR) in doubly-fed induction generator (DFIG)-based wind farms*. Springer Nature, 2022.

[15] K.-H. Kim, T. L. Van, D.-C. Lee, S.-H. Song, and E.-H. Kim, "Maximum output power tracking control in variable-speed wind turbine systems considering rotor inertial power," *IEEE transactions on industrial electronics*, vol. 60, no. 8, pp. 3207–3217, 2012.

[16] M. Wu, L. Xie, L. Cheng, and R. Sun, "A study on the impact of wind farm spatial distribution on power system

sub-synchronous oscillations," *IEEE Transactions on Power Systems*, vol. 31, no. 3, pp. 2154–2162, 2015.

[17] M. Wu and L. Xie, "Calculating steady-state operating conditions for dfig-based wind turbines," *IEEE Transactions on sustainable Energy*, vol. 9, no. 1, pp. 293–301, 2017.

[18] M. Abdeen, H. Li, and L. Jing, "Improved subsynchronous oscillation detection method in a dfig-based wind farm interfaced with a series-compensated network," *International Journal of Electrical Power & Energy Systems*, vol. 119, p. 105930, 2020.

[19] L. Fan and Z. Miao, "Mitigating ssr using dfig-based wind generation," *IEEE Transactions on Sustainable Energy*, vol. 3, no. 3, pp. 349–358, 2012.

[20] A. K. Abdulabbas, M. A. Alawan, and D. K. Shary, "Limits of reactive power compensation of a doubly fed induction generator based wind turbine system," *Bulletin of Electrical Engineering and Informatics*, vol. 12, no. 5, pp. 2521–2534, 2023.

[21] M. R. A. Pahlavani and H. A. Mohammadpour, "Damping of sub-synchronous resonance and low-frequency power oscillation in a series-compensated transmission line using gate-controlled series capacitor," *Electric Power Systems Research*, vol. 81, no. 2, pp. 308–317, 2011.

[22] L. Piyasinghe, Z. Miao, J. Khazaei, and L. Fan, "Impedance model-based ssr analysis for tcsc compensated type-3 wind energy delivery systems," *IEEE Transactions on Sustainable Energy*, vol. 6, no. 1, pp. 179–187, 2014.

[23] Y. Lei, A. Mullane, G. Lightbody, and R. Yacamini, "Modeling of the wind turbine with a doubly fed induction generator for grid integration studies," *IEEE transactions on energy conversion*, vol. 21, no. 1, pp. 257–264, 2006.

[24] F. Mei and B. Pal, "Modal analysis of grid-connected doubly fed induction generators," *IEEE transactions on energy conversion*, vol. 22, no. 3, pp. 728–736, 2007.

[25] L. Fan, C. Zhu, Z. Miao, and M. Hu, "Modal analysis of a dfig-based wind farm interfaced with a series compensated network," *IEEE Transactions on Energy Conversion*, vol. 26, no. 4, pp. 1010–1020, 2011.

APPENDIX

TABLE VIII.
DFIG PARAMETERS

Parameters	Single generator	Wind frame
Rated power	2MW	100MW
Rated voltage	575 V	575 V
Rated frequency	60 Hz	60 Hz
rs_s	0.023p.u.	
X_{ls}	0.18p.u.	
R_R	0.016p.u.	
X_l	0.16p.u.	
X_m	2.9p.u.	1200 V
Dc-link voltage	1200 V	$50^{*}10000\mu$F
DC-link capacitor	10000μF	100MW
Base power	2MW	
Base voltage	575 V	

TABLE IX.
TRANSMISSION LINES PARAMETERS

Transformer ratio	575 V/161 kV
Rated power	100MW
Rated voltage	161kV
Rated frequency	60 Hz
R_{im}	0.02pu
X_{din}	0.5pu
X_{ovown} at 50% of Com. level	64.8Ω
X_T	0.14pu
X_{ow}	0.06pu